MICROBOONE-NOTE-1003-PUB

Measurement of the Electronegative Contaminants and Drift Electron Lifetime in the MicroBooNE Experiment

The MicroBooNE Collaboration

May 19, 2016

Abstract

High-purity liquid argon is critical for the operation of a liquid argon time projection chamber (LArTPC). At MicroBooNE, we have achieved an electron drift lifetime of at least 6 ms without evacuation of the detector vessel. Measurements of the electronegative contaminants oxygen and water are described and shown as the gas and liquid argon stages of filtration progressed.

1 Introduction

MicroBooNE, being a liquid argon time projection chamber (LArTPC) detector, requires high-purity liquid argon to operate. High-purity is defined as having a sufficiently low-level of electronegative contamination to provide electron drift lifetimes greater than 3 ms. To obtain the needed high-purity liquid argon, we repeated the procedure originally performed by the Liquid Argon Purity Demonstrator (LAPD) [1], also forgoing the evacuation of the detector volume prior to filling with liquid argon. The process involved four steps: a gaseous argon "piston" purge, recirculation of the gaseous argon through a molecular sieve to remove water, filling of the vessel with liquid argon, and recirculation of the liquid through the filtration system.

MicroBooNE began with the gaseous argon purge on April 20, 2015. MicroBooNE continued with purification of its liquid argon on July 24, 2015. This document describes and demonstrates the cleanup of the liquid argon as the gaseous purge and liquid filtration progressed.

MicroBooNE has two pairs of filters which focus on removing electronegative contaminants which impact the electron drift lifetime. Each pair consists of two filter vessels, one for filtering water and the other for oxygen. The water filter vessels are filled with 4A molecular sieves supplied by Sigma-Aldrich [5]. The oxygen filter vessels are filled with BASF CU-0226 S, a dispersed copper oxide impregnated on a high surface area alumina [6]. Although these filters remove oxygen and water, the filters were measured to contain radioactive impurities from the decay chains of thorium-232 and uranium-238. The impact of these radioactive impurities on detector operation is under active investigation by the experiment.

2 Purity Measurement from Gas Analyzers

2.1 Gas Analyzers

MicroBooNE has five gas analyzers for measuring contaminants in the liquid. The electronegative contaminants oxygen and water absorb signal electrons created from the ionization of argon atoms. The other contaminant of note is nitrogen, which disrupts scintillation light via absorption and quenching. For measuring the concentration of oxygen, we use two Servomex gas analyzers, a DF-310E and a DF-560E [2]. Together, the analyzers cover a range of 0.1 parts-per-billion (ppb) to 5000 parts-per-million (ppm). To measure the level of water contamination, we use a Tiger Optics Halo+ gas analyzer [3] and a Vaisala dew point sensor [4]. MicroBooNE's gas analyzer system has the capability of taking measurements at multiple points around the cryogenics system.

2.2 Gaseous Argon Purge

We began operations with a "piston" purge, introducing argon gas through sparger holes in the bottom of the cryostat. Assuming that the argon gas has a density higher than the initial gas mixture in the cryostat, the argon gas acts similarly to a piston in pushing the initial gas mixture up and out.

For the measurements of the purge, the analyzers were sampling from a gas vent on the cryostat containing the detector. We estimate the initial contamination of oxygen in the cryostat to be roughly 1% as the vessel was filled with nitrogen gas for a pressure test. We also estimate that it took 10 hours to perform a complete volume exchange of the gas in the system. The drop in oxygen and water concentrations as the purge progressed from April 20 to April 26 appears in Fig. 1. The data in the plots come from the low-sensitivity DF-310E sensor and the Vaisala dew point sensor. Oxygen concentration measurements began on the second day of the purge or around hour 24. Initially, the oxygen concentration of roughly 1% was out of the range of the DF-310E analyzer. After one day, it was low enough for the analyzer to measure. In the oxygen curve, a bump appears around hour 55 which is believed to have been caused by the release of trapped air from inside the vessel.

The purge produces a front of argon gas, the top of the "piston", that moves from the bottom of the cryostat to the top. When the argon front hits a level in the cryostat, the oxygen and water concentrations drop sharply. The initial "piston" purge occurs on the timescale of roughly one volume exchange over which the argon front moves from the bottom of the cryostat to the top. In Fig. 1, the water and oxygen analyzers were inactive during the initial volume exchange. After the argon front has passed through the vessel, the flow of argon gas into the cryostat continued, further acting to push the lighter ambient air out.

After the front passes and before hour 25, the buoyant advantage of the argon gas over the ambient air is gradually lost in the cryostat. The loss is not uniform throughout the cryostat, occurring at different locations in the cryostat at different times. At hour 25, after about two volume exchanges, the buoyant advantage is lost nearly throughout the entire volume. The effects of water outgassing and mixing of the gasses in the cryostat then become dominant, resulting in the kink that appears at hour 25. The timescale of the drop in water concentration when water outgassing and

mixing dominate (after hour 25) is much larger than the timescale when the "piston" purge is active over the first two volume exchanges. After hour 25, mixing the argon with gasses in the cryostat and then venting the mixture is the only way to reach a higher purity. As expected then, the decrease in contamination is observed to be faster using the "piston" purge than it would have been with perfect mixing of the ambient air and argon.

In Fig. 1, a gap in the water concentration curve around hour 80 to hour 100 is due to a pressure test of the MicroBooNE cryostat. During this test, purging and filtration processes were paused. The pressure of the vessel was increased to 8 psig to verify that the vessel and its connections were leak tight. Pausing the purge for the test resulted in a higher water concentration due to outgassing at hour 100, when we resumed purging.

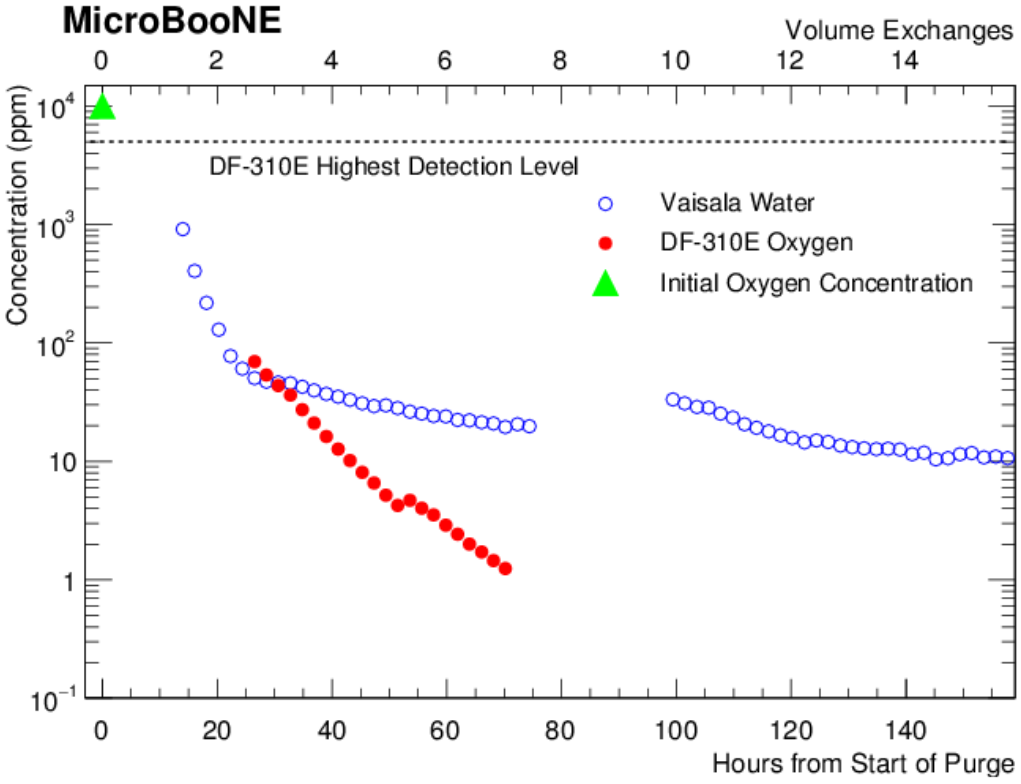

Figure 1: A plot of the oxygen and water concentrations as the gaseous argon purge progressed. We estimate the initial oxygen concentration as being roughly 1% and indicate that point with the green marker. The initial oxygen concentration was out of range of the DF-310E sensor. As a result, its curve does not begin until after 24 hours into the purge. The sharp decrease of the water concentration between hours 10 and 25 occurs when the buoyant action of the argon gas purge is still dominant. After hour 25, outgassing of water and mixing of gasses in the cryostat becomes dominant. The bump that appears in the oxygen curve at hour 55 is believed to have resulted from air trapped inside the vessel escaping. A gap in the water curve appears around hour 80 due to a pressure test of the vessel that lasted until hour 100. Due to outgassing of water during the test, the water concentration is at a higher concentration when the purge resumed at hour 100.

2.3 Liquid Argon Filtration

The process of the removal of water and oxygen contamination from the liquid as filtration started on July 24, 2015 and continued for two weeks appears in Fig. 2. We produced the oxygen contamination curve using data from the more sensitive DF-560E analyzer. The oxygen concentration curves begin at 12 hours and the water curve begins one day after the start of filtration. This is due to both sensors undergoing calibrations. As is visible in the figure, the oxygen concentration reaches the analyzer's lowest sensitivity just prior to day 7. The water concentration eventually reached the lower limit of the HALO+'s sensitivity.

The full range of the HALO+ is 0–20 parts-per-million (ppm) with the lower detection limit of 2 ppb. Prior to day 5, the concentration range was set to 0–1000 ppb, after day 5 the concentration range was lowered to 0–100 ppb as the argon cleaned up. The discontinuity on day 5 is a result of the change in concentration output range and a small range error due to the PLC.

As the water concentration hits the lower detection limit of the HALO+, the concentration demonstrates some waviness. This likely results from the analyzer reaching the bottom of its range where measurement uncertainties abound. Another possibility is that outgassing from inside of the line running from the sample point to the analyzer itself, causing it to vary with the ambient temperature.

For the measurements of the liquid filtration, the analyzers were sampling at the discharge point of the liquid argon pumps, upstream of the filters. The pumps take liquid from the cryostat and from the condensers and then moves the argon through the oxygen and water filters.

3 Purity Measurement from Purity Monitors

3.1 Purity Monitors at MicroBooNE

MicroBooNE has three purity monitors to measure electronegative contamination beyond the ranges of the gas analyzers. Purity monitors are double-gridded ion chambers immersed in liquid argon. The MicroBooNE purity monitors are based on the design in Ref. [7]. MicroBooNE uses purity monitors and data acquisition hardware and software nearly identical to that used at the Liquid Argon Purity Demonstrator (LAPD) [1]. The monitors themselves contain four circular electrodes, all parallel to each other. The first is a photocathode, supported by a stainless steel disk. The second and third are open wire grids, acting as cathodes and anodes respectively. The fourth is a stainless steel disk acting as an anode. A drawing and a schematic of a purity monitor appears in Fig. 3.

The cathode wire grid is held at a ground potential. The cathode, anode grid, and anode are accessible via a modified high voltage vacuum grade feed-through port. The anode and cathode grids are separated by field-shaping rings, with the anode grid connected to the cathode grid by a resistor chain of 50 MΩ resistors. This provides a uniform electric field in the volume between the two grids. Of great importance is the transparency of the grid wires to electrons passing through them. To provide maximum transparency [8], we use field ratios that satisfy

$$E_1 > 2E_2 > 4E_3, \tag{1}$$

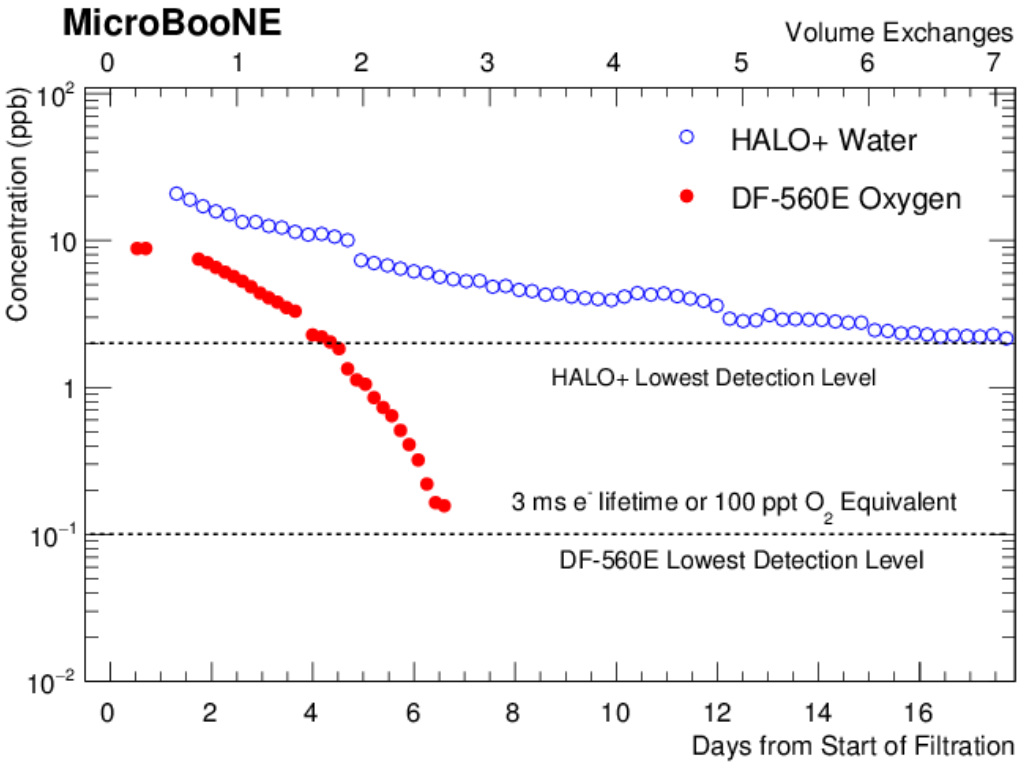

Figure 2: A plot of the oxygen and water concentrations as filtration of the liquid phase argon began and continued for two weeks. The lower range of the oxygen analyzer was reached just prior to day 7. The discontinuity in the water concentration occurring around day 5 is due to the HALO+ switching sensitivity mappings. Both the DF-560E oxygen and HALO+ water analyzers were undergoing calibrations when filtration began. As a result, the data for both analyzers begins a few hours to a day after filtration began.

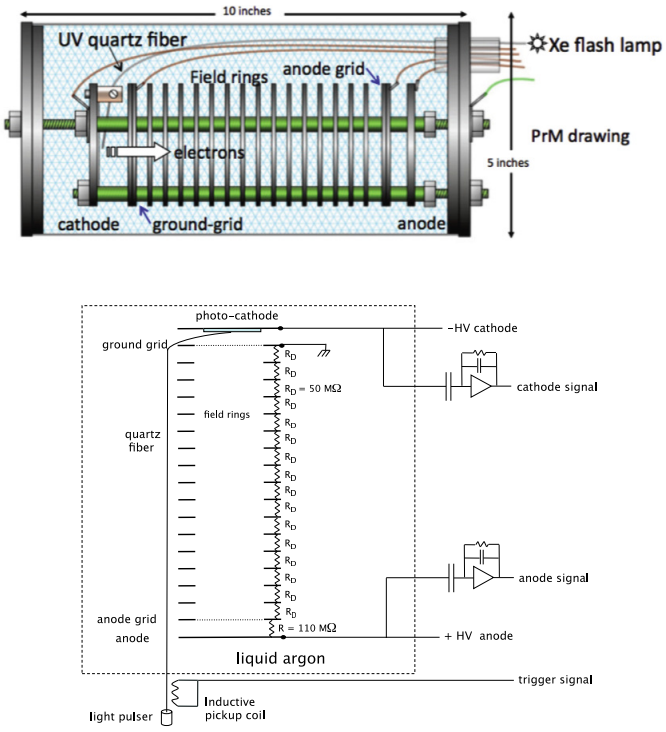

Figure 3: A drawing (top) of a purity monitor and a schematic (bottom) of one. The drawing and schematic are sourced from [1].

where E_1 is the field between the anode grid and the anode; E_2 is the field between the anode grid and the cathode grid; and E_3 is the field between the cathode and the cathode grid.

Our purity monitors use a 2.54 cm $\times$ 3.18 cm $\times$ 0.8 mm aluminum plate coated with 5 nm of titanium and 100 nm of gold as the photocathode fixed to the cathode disk. To supply light to the photocathode, we use a xenon flash-lamp external to the cryostat to produce UV light that is then steered to the photocathode using three quartz fibers, each 0.6 mm in diameter. The quartz fiber used is FDP600660710 from Polymicro Technologies [9].

When the flash-lamp is fired, UV light frees electrons from the photocathode that then drift towards the cathode grid. The freed electrons induce a current on the cathode. After passing through the cathode grid, the electrons experience the field from the anode grid. The anode and cathode wire grids act to prevent induced currents from appearing on the cathode or anode while the electrons are flowing through the drift volume. Once past the anode grid, the electrons then induce a current on the anode. The induced currents on the anode and cathode are then amplified and integrated.

MicroBooNE has two of the three purity monitors inside the cryostat and one monitor inside of an inline vessel downstream of the liquid argon filters. The two inside-the-cryostat monitors are of differing lengths and therefore offer different electron drift distances. A short purity monitor sits near the bottom of the cryostat and has a total drift distance of 19 cm. The other monitor inside of the cryostat has a total drift distance of 50 cm and will henceforth be referred to as the long purity monitor. Due to

difficulties during commissioning, only data from the long purity monitor is reported in this note.

3.2 Purity Monitor Analysis

To gain understanding of the level of electronegative contamination present, we look at the charge arriving at the anode (Q_A) after a drift time t_{drift} to that leaving the cathode (Q_C). We measure Q_C and Q_A by integrating the induced charge at the cathode and anode respectively. The ratio of Q_A/Q_C can be interpreted as an electron lifetime τ using the relation

$$Q_A/Q_C = e^{-t_{drift}/\tau}. \tag{2}$$

Following the analysis described in Ref. [1], we look for the maximum pulse heights, V_{max}, of the anode and cathode oscilloscope traces. An example set of traces for the long purity monitor, taken on the morning of August 17, appears in Fig. 4. Walking through the calculation shown in Fig. 4, the flash-lamp fires at 0.5 ms and the cathode peak appears shortly thereafter at 0.62 ms. The cathode peak is measured to be -6.02 mV and is labeled (b) in Fig. 4. The anode maximum pulse height is determined to be 6.11 mV, appearing at 3.32 ms. The anode pulse maximum is labeled (d) in Fig. 4. Both of the anode and cathode peaks are considered raw as they are not yet corrected for baselines or electronics response.

The calculation moves ahead with the determination of the baselines. For the cathode, we look right before the cathode pulse at 0.250 ms, labeled (a) in Fig. 4. We average 50 samples about the 0.250 ms point, 25 samples at and before 0.250 ms and 25 samples after 0.250 ms. The low frequency sinusoidal noise makes determination of the anode baseline difficult. To determine it, we look at a sample 0.083 ms before the start of the anode pulse to mitigate the noise. The point sampled for the anode baseline is also labeled (c) in Fig 4. Going right in front of the anode pulse helps to decrease the impact of the low frequency noise.

A version of the oscilloscope traces appears in Fig. 5 with labels for drift time from anode to cathode, cathode amplifier circuit discharge (bleed-off), anode amplifier circuit discharge (bleed-off), and charge arrival at anode.

We apply a correction to the pulse heights of the cathode and anode signals to account for the fact that the integrating circuit has a discharge time that is not long in comparison to the signal rise time. This has the effect of reducing the peak for a given total charge by an amount that depends on the signal rise time.We approximate the photoelectron signal on the anode and cathode as a square pulse of duration Δt. The electronics respond as an RC circuit with a time constant of $RC = 119$ µs. With the assumption of a square pulse and RC circuit response, the pulse heights receive a correction factor for the electronics of

$$f(\Delta t, RC) = \frac{\Delta t}{RC} \frac{1}{1 - \exp(-\frac{\Delta t}{RC})}. \tag{3}$$

We use the rise time of the pulses for Δt. The cathode and anode correction factors are determined to be 1.6 and 1.3 respectively.

We can then calculate the charge seen by the cathode and anode using

$$Q = (V_{max} - V_0) \times f(\Delta t, RC). \tag{4}$$

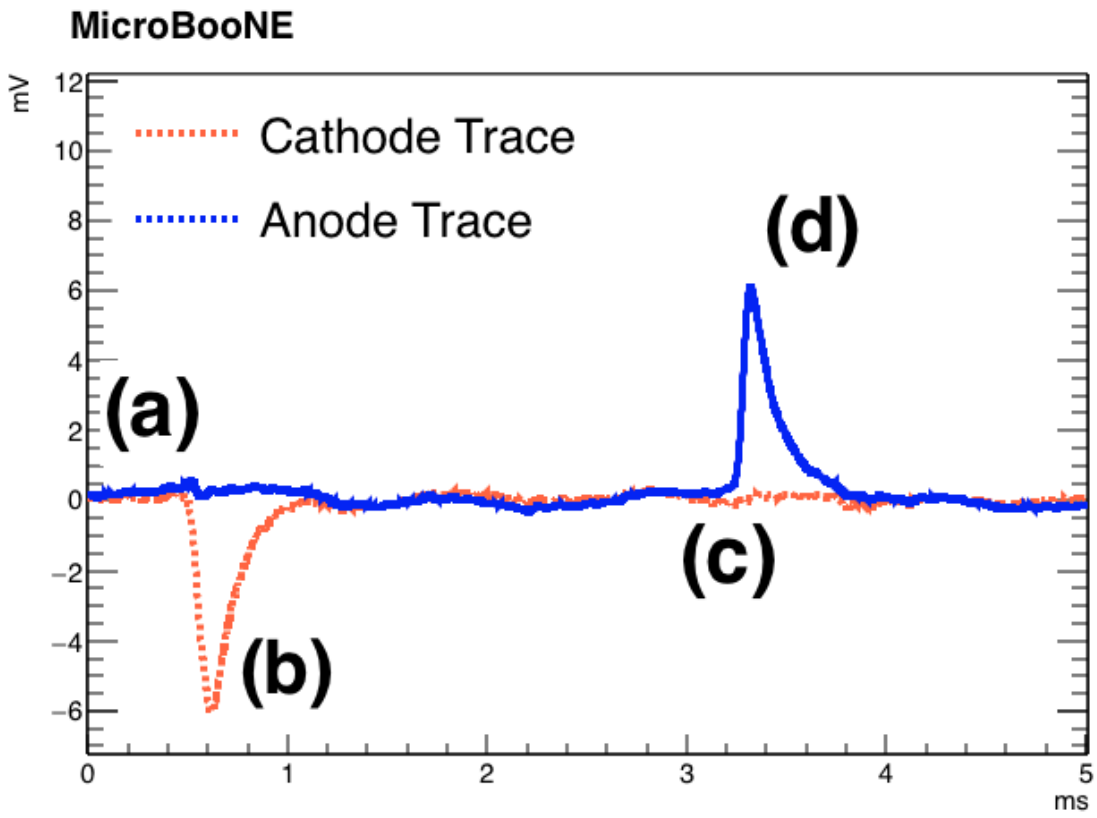

Figure 4: A plot of the oscilloscope traces from data taken with the long purity monitor on the afternoon of September 17. Both the traces before and after noise subtraction appear. The data produced a lifetime measurement of 8.4 ms. The cathode pulse maximum (b) and the point (a) where its baseline is determined are labeled. For the anode, the pulse maximum (d) and the baseline sample point (c) are also labeled. The waviness seen in the traces is suspected to arise from HV power supply ripple. The fall time of the pulses indicates the discharge time of the integrating circuit as mentioned in the text.

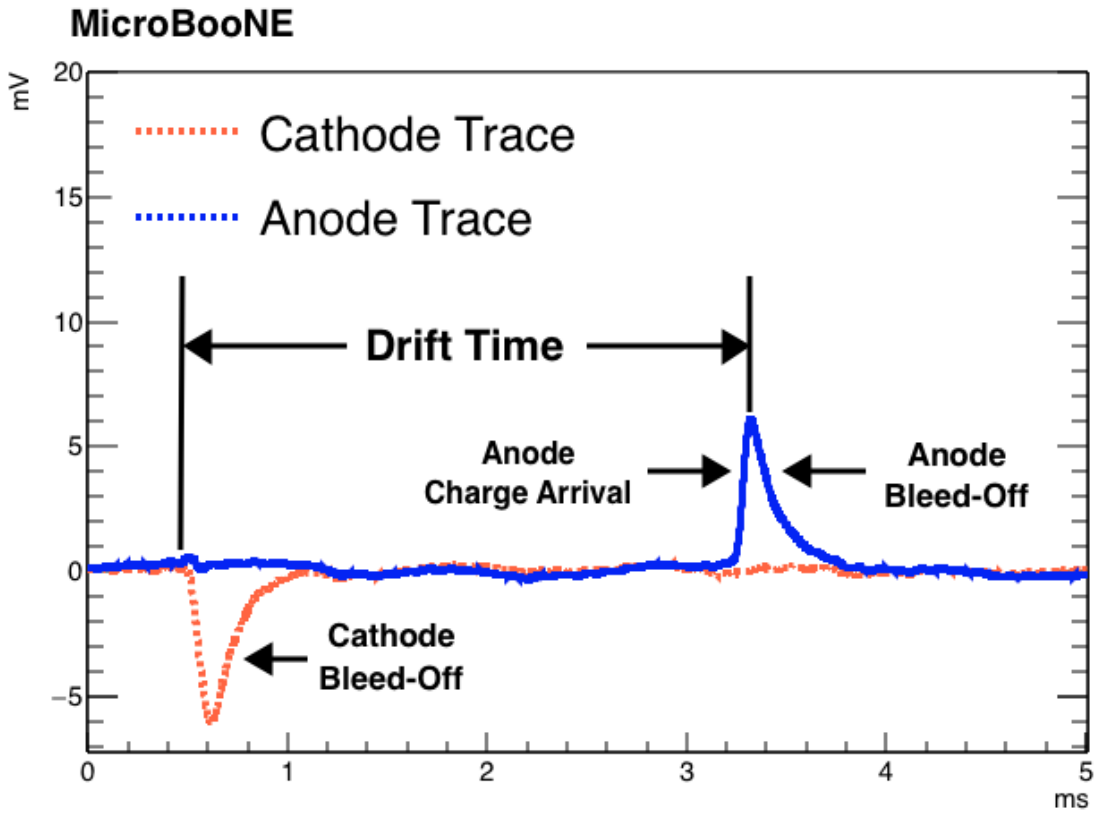

Figure 5: A plot of the oscilloscope traces from data taken with the long purity monitor on the afternoon of September 17 labeled for the drift time of 2.82 ms, the charge arrival at the anode, and the capacitor discharge (bleed-off) for both the cathode and anode.

The drift time is determined from taking the difference between the time of the anode peak at 3.32 ms and the trigger time of 0.5 ms, resulting in 2.82 ms. Using the drift time of 2.82 ms, a lifetime can be determined via Eqn. 2. For this trace, a value of 8.4 ms is found.

We plot the ratio of Q_A/Q_C for the long purity monitor from August 5 to August 19 as liquid argon filtration continued in Fig. 6. For electron lifetime estimation, we draw lines corresponding to lifetimes of 3 ms, 6 ms, and 9 ms on the plot. MicroBooNE measured and achieved an electron lifetime of at least 6 ms or less than 50 parts-per-trillion (ppt) oxygen equivalent contamination. As described in Ref. [1], the electron lifetime derived from purity monitors is best thought of as a lower limit as systematic uncertainties serve to increase the lifetime and not reduce it.

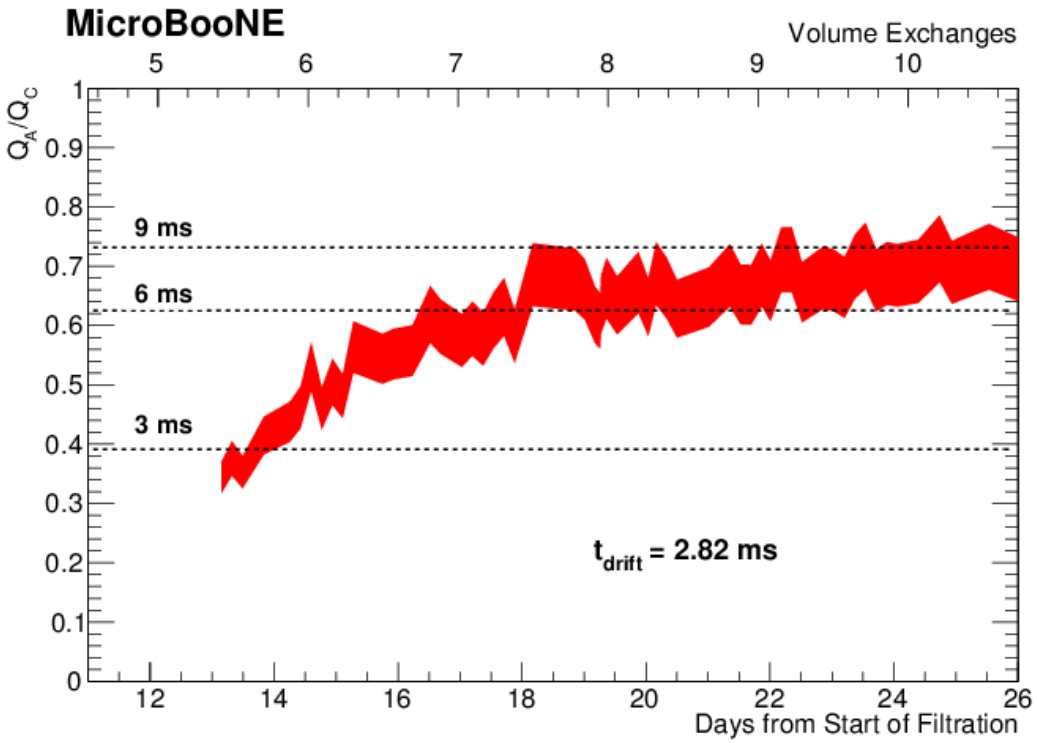

Figure 6: A plot of Q_A/Q_C from the long purity monitor as liquid argon filtration continued at MicroBooNE for $t_{drift} = 2.82$ ms. Lines for lifetimes of 3 ms, 6 ms, and 9 ms are also drawn for their respective values of Q_A/Q_C. The uncertainty is shown as the red error band corresponding to $\pm 7.8\%$. The design requirement for operation of the detector is 3 ms.

3.3 Systematic Uncertainties

There are several sources of systematic uncertainties that we explored for this analysis. For statistical uncertainty, we found a standard deviation for a series of Q_A/Q_C taken when the purity to be 3%.

As described in Ref. [1], there is a correction applied to account for differences in the amplifiers used for the anode and cathode. That correction factor to be applied to the Q_A/Q_C ratio was found to be 1.007 ± 0.007. The correction factor has been applied for data in the Q_A/Q_C plot.

Due to low-frequency noise appearing in the oscilloscope traces for the anode, the baseline determination becomes a large systematic uncertainty. Two techniques were explored for determining the baseline for the anode pulses. First, the default approach, we took the baseline right before the anode pulse as mentioned above. Second, 400 points were sampled half-way between the anode and cathode pulses on the anode trace. The second technique produced a 5.7% larger value of the ratio. A systematic uncertainty of 5.7% was then applied to all values of Q_A/Q_C.

The last uncertainty examined was due to the measured value of the RC constant used to determine the electronics response correction. Several measurements of RC were made and applied to the analysis. A systematic uncertainty of 4.1% was applied to Q_A/Q_C.

The total statistical and systematic uncertainty was taken to be 7.8%, appearing as an error band in Fig. 6.

Reference [1] notes three additional sources of systematic uncertainties involved in the purity measurement. First, we assume that the acceptance on the anode is 100%. If the anode acceptance is less than 100%, then a number of photoelectrons from the cathode will traverse the full drift distance without encountering an impurity and yet not be measured by the anode. This leads to a lower value of Q_A and a lowered measured ratio of Q_A/Q_C.

Second, a photoelectron moving from the cathode to the cathode grid may be absorbed by an impurity before moving past the cathode grid and into the drift volume. This photoelectron will still produce a signal on the cathode however. This will lead to an inflated value of Q_C and a lowered measured value of Q_A/Q_C.

Third, the value of RC may be larger than the value used for the analysis of 119 µs. The cathode is impacted more by a change in the value of RC. If the value of RC is larger than 119 µs, the correction factor of $f(\Delta t, RC)$ is smaller that if it were calculated using 119 µs. This has the effect of decreasing the values of both Q_A and Q_C. Since Q_C is impacted more than Q_A though by this change, this results in increasing the ratio of Q_A/Q_C. The choice of using $RC = 119$ µs allows the value of Q_A/Q_C to be lower than it likely is.

All three of the systematics reported by [1] have the impact of lowering the measured ratio of Q_A/Q_C and thus lowering the measured lifetime. For this reason, the lifetime values we quote are best considered a lower limit on the true lifetime.

4 Conclusions

This document details measurements of oxygen and water contamination demonstrating that the MicroBooNE cryogenics system successfully achieved liquid argon with

levels of those two contaminants low enough to allow for operation of the experimental program without vessel evacuation. The measurements show oxygen and water being removed from the system beginning with a gaseous purge and progressing through the filtering of liquid argon. After the process was complete, an electron drift lifetime equal to or greater than 6 ms was measured. The 6 ms lifetime corresponds to an oxygen equivalent contamination of less than 50 ppt. The 6 ms lifetime exceeds the design specification of equal to or greater than 3 ms.

5 Acknowledgements

The authors would like to acknowledge the contributions of Ron Davis, Alan Hahn, Walter Jaskierny, and Mark Ruschman. All provided invaluable assistance in bringing the purity monitors online successfully.

References

[1] M. Adamowski *et al.*, "The Liquid Argon Purity Demonstrator," *JINST* **9** (2014) P07005, `arXiv:1403.7236 [physics.ins-det]`.

[2] Spectris plc, Heritage House, Church Road, Egham, TW20 9QD, United Kingdom.

[3] Tiger Optics LLC, 250 Titus Ave, Warrington, PA, 18976-2426.

[4] Vaisala Oyj, P.O. Box 26, FI-00421 Helsinki, Finland.

[5] Sigma-Aldrich, P.O. Box 14508, St. Louis, MO 63178 USA.

[6] BASF Corp., 100 Park Avenue, Florham Park, NJ 07932 USA.

[7] G. Carugno *et al.*, "Electron lifetime detector for liquid argon," *Nucl. Instrum. Meth. A* **292** (1990) 580.

[8] O. Bunneman, B. Cranshaw, and J.A. Harvey, Can J. Res. *27*, 191 (1949).

[9] Polymicro Technologies 18019 N 25th Ave, Phoenix, AZ 85023.